Physica Medica 103 (2022) 37–45

Contents lists available at ScienceDirect

Physica Medica

journal homepage: www.elsevier.com/locate/ejmp

Multi-centre and multi-vendor reproducibility of a standardized protocol for quantitative susceptibility Mapping of the human brain at 3T

Marta Lancione [a,1], Paolo Bosco [a,1], Mauro Costagli [a,b], Anna Nigri [c], Domenico Aquino [c], Irene Carne [d], Stefania Ferraro [c,e], Giovanni Giulietti [f,g], Antonio Napolitano [h], Fulvia Palesi [i,j], Luigi Pavone [k], Alice Pirastru [l], Giovanni Savini [m], Fabrizio Tagliavini [n], Maria Grazia Bruzzone [c], Claudia A.M. Gandini Wheeler-Kingshott [i,j,o], Michela Tosetti [a,*], Laura Biagi [a], the RIN – Neuroimaging Network

[a] Laboratory of Medical Physics and Magnetic Resonance, IRCCS Stella Maris Foundation, Pisa, Italy
[b] Department of Neuroscience, Rehabilitation, Ophthalmology, Genetics, Maternal and Child Sciences (DINOGMI), University of Genoa, Genoa, Italy
[c] Neuroradiology Unit, Fondazione IRCCS Istituto Neurologico Carlo Besta, Milan, Italy
[d] Neuroradiology Unit, IRCCS Istituti Clinici Scientifici Maugeri, Pavia, Italy
[e] MOE Key Laboratory for Neuroinformation, School of Life Science and Technology, University of Electronic Science and Technology of China, Chengdu, China
[f] Neuroimaging Laboratory, IRCCS Santa Lucia Foundation, Rome, Italy
[g] SAIMLAL Department, Sapienza University of Rome, Rome, Italy
[h] Medical Physics, IRCCS Istituto Ospedale Pediatrico Bambino Gesù, Rome, Italy
[i] Neuroradiology Unit, IRCCS Mondino Foundation, Pavia, Italy
[j] Department of Brain and Behavioral Sciences, University of Pavia, Pavia, Italy
[k] IRCCS Neuromed, Pozzilli, Italy
[l] IRCCS Fondazione Don Carlo Gnocchi Onlus, Milan, Italy
[m] Neuroradiology Unit, IRCCS Humanitas Research Hospital, Milan, Italy
[n] Scientific Direction, Fondazione IRCCS Istituto Neurologico Carlo Besta, Milan, Italy
[o] NMR Research Unit, Department of Neuroinflammation, Queen Square MS Centre, UCL Queen Square Institute of Neurology, Faculty of Brain Sciences, University College London, London, United Kingdom

ARTICLE INFO

Keywords:
Magnetic resonance imaging
Quantitative susceptibility mapping
Multicentric study
Protocol harmonization
Reproducibility

ABSTRACT

Quantitative Susceptibility Mapping (QSM) is an MRI-based technique allowing the non-invasive quantification of iron content and myelination in the brain. The RIN – Neuroimaging Network established an optimized and harmonized protocol for QSM across ten sites with 3T MRI systems from three different vendors to enable multicentric studies. The assessment of the reproducibility of this protocol is crucial to establish susceptibility as a quantitative biomarker. In this work, we evaluated cross-vendor reproducibility in a group of six traveling brains. Then, we recruited fifty-one volunteers and measured the variability of QSM values in a cohort of healthy subjects scanned at different sites, simulating a multicentric study. Both voxelwise and Region of Interest (ROI)-based analysis on cortical and subcortical gray matter were performed.

The traveling brain study yielded high structural similarity (~0.8) and excellent reproducibility comparing maps acquired on scanners from two different vendors. Depending on the ROI, we reported a quantification error ranging from 0.001 to 0.017 ppm for the traveling brains. In the cohort of fifty-one healthy subjects scanned at nine different sites, the ROI-dependent variability of susceptibility values, of the order of 0.005–0.025 ppm, was comparable to the result of the traveling brain experiment.

The harmonized QSM protocol of the RIN – Neuroimaging Network provides a reliable quantification of susceptibility in both cortical and subcortical gray matter regions and it is ready for multicentric and longitudinal clinical studies in neurological and pychiatric diseases.

* Corresponding author.
E-mail address: michela.tosetti@fsm.unipi.it (M. Tosetti).
[1] These authors contributed equally to this work.

https://doi.org/10.1016/j.ejmp.2022.09.012
Received 7 June 2022; Received in revised form 12 September 2022; Accepted 27 September 2022
Available online 8 October 2022

Introduction

The understanding of the pathological pattern of iron deposition and its causal relationship with neuronal loss is a crucial issue for the study of neurodegeneration [1,2]. Non-invasive in-vivo quantification of iron stores can be performed using Quantitative Susceptibility Mapping (QSM), an advanced MRI technique [3–5]. QSM measures magnetic susceptibility (χ), which is an inherent magnetic property of tissues, from the phase signal obtained by Gradient Recalled Echo (GRE) acquisitions. The static magnetic field B_0 of the MRI scanners induces a magnetization in tissues containing paramagnetic molecules, such as ferritin, or diamagnetic substances, like myelin or calcium, which in turn generate dipolar field perturbations. These perturbations lead to two main effects: on the one hand, transverse T2* relaxation is accelerated causing a faster decay of signal intensity; on the other hand, the phase of the signal accrues linearly with the dipolar field distortion. QSM aims at deconvolving the dipole field kernel which characterizes this perturbation in order to retrieve information on the susceptibility sources generating the perturbation, resulting in a quantitative and local map of magnetic susceptibility.

The histological validation of QSM, showing the correlation of measured susceptibility with iron concentration and myelination, together with the ease of implementation as no dedicated hardware or sequence are required, increased QSM popularity and its application to a variety of disorders [6,7], e.g. Parkinson's disease [8–11], Amyotrophic Lateral Sclerosis [12–14] or Alzheimer's diseases [15–18], and pioneered the use of QSM as a quantitative MRI biomarker. However, an MRI biomarker should be fully quantitative to make an impactful contribution to the diagnosis, prognosis, and follow-up of patients, both during the natural history of pathology and during treatments. The assessment of its reliability in time and space is fundamental to evaluate the reproducibility of results in longitudinal and in multi-center/multi-vendor studies.

The impact of mono-centric studies is limited by the small cohorts recruited for research purposes, especially for low-prevalence diseases such as atypical Parkinsonism (e.g. Multiple System Atrophy), Friedreich ataxia or Huntington's disease. The optimization and the harmonization of acquisition protocols across a wide network of hospitals and research centers would enable the enrollment of larger populations of patients and a more comprehensive study of risk factors and other relevant clinical variables. However, susceptibility measured via QSM was shown to depend on several experimental factors including both fundamental physical properties of susceptibility and acquisition parameters. Magnetic susceptibility could be more rigorously modeled as a second-order tensor and its estimation would require at least six acquisitions with the patient's head oriented differently with respect to the main static magnetic field B_0 [19–21]. As this is not feasible in clinical practice due to patient discomfort and long scanning time, QSM approaches approximate susceptibility to a scalar quantity. This leads to χ dependence on head orientation, especially in highly organized structures such as white matter fiber bundles where myelin sheath microstructure is responsible for susceptibility anisotropy, while this should not represent a confounding factor in gray matter [22]. Acquisition parameters affecting χ quantification are spatial resolution [23,24], brain coverage [23,25], echo time [26–30] and field strength [29,31,32]. For this reason, multicentric studies require careful optimization and standardization of the GRE sequence used to perform QSM across clinical systems from different vendor platforms and the assessment of the reproducibility of the biomarkers of interest.

Previous studies assessed QSM reproducibility in multi-centric studies at 1.5 T, 3T and 7 T using scanner platforms from one [29,31,33–35] or two vendors [36–38]. Good reproducibility was reported for repeated scans on the same system and for standardized protocols across scanners operating at the same field strength, while to obtain consistent results at different field strengths required careful optimization of echo times [29].

The RIN – Neuroimaging Network (https://www.reteneuroscienze.it/en/progetti/neuroimaging/) aimed at creating a harmonized protocol, including a GRE sequence for QSM, and at setting it up on several clinical 3T MRI scanners from three vendors, in order to be able to aggregate data and boost our knowledge on brain structure and function in physiological and pathological conditions.

In this study, a harmonized multi-echo GRE sequence was acquired at ten different sites across Italy on a population of healthy adults. In addition, four sites were involved in a "traveling brain" experiment in which six volunteers were scanned on 3T MRI systems from different vendors. We performed voxel-wise and ROI-based analyses on both cortical and subcortical structures to assess the similarity of the maps and the reproducibility of χ maps. We also provided an estimation of the susceptibility variability that can be expected over a healthy population for inter-site, inter-vendor or cross-vendor acquisitions.

Methods

Experimental design

This study involved sites of the RIN - Neuroimaging Network equipped with 3T MRI scanners and data were acquired on scanner platforms from three vendors (Philips, Siemens and GE Healthcare).

For the traveling brain experiment, four sites located in two different areas of Italy (two in area A1 and two in A2) with scanners from two different vendors (V1 and V2) were selected. Three healthy subjects (S1-3; 1 female and 2 males, 29, 30 and 33 years old) were scanned at both A1 sites and three other subjects (S4-6; 2 females and 1 male, 21, 21 and 43 years old) at both A2 sites, so that each subject was scanned once for vendor V1 and once for V2. This information is summarized in Table 1.

To assess inter-site variability on a healthy population, fifty-one volunteers (33 females and 18 males, 29 ± 5 [21–40] years old) underwent a 3T MRI scan in one of nine sites with MR systems from three different vendors (V1, V2, V3): five sites from V1, three sites from V2 and one from V3. Demographic and technical information on the subject cohort and the MRI system of each site are reported in Table 2.

The participants had no history of neurological diseases or psychiatric disorders and gave their written informed consent. The Protocol Study was performed under the Declaration of Helsinki (59th General Assembly of the World Medical Association, Seoul, October 2008) and the Medical Research Involving Human Subjects Act (WMO). All the procedures described were performed in compliance with security, integrity, and privacy. The studies involving human participants were reviewed and approved by the Ethics Committee of Lombardy Region - IRCCS Institute of Neurology Carlo Besta Foundation Section.

MRI imaging protocol

The MRI protocol was optimized and standardized across sites on 3T MRI platforms from three different vendors [39], in order to minimize inter-vendor differences in acquisition parameters. The Standard Operating Procedures (SOPs) required that subjects be positioned inside the scanner so that the bicallosal alignment and the pure axial alignment corresponded, to minimize the effect of different head orientations across subjects. For susceptibility mapping, a flow-compensated 3D

Table 1
Details on the hardware and the cohort of traveling brains for each site involved in the study.

Area	Site	Vendor	Coil [ch]	Subjects	Age [y]	Sex
A1	1	V1	32	3	29, 30, 33	1F/2M
	2	V2	64			
A2	3	V1	32	3	21, 21, 43	2F/1M
	4	V2	32			

Table 2
Details on the hardware and the cohort of healthy subjects for each site involved in the study.

Site	Vendor	Coil [ch]	Subjects	Age [y]	Sex
1	V1	32	5	32 ± 2	3F/2M
2	V1	32	6	30 ± 4	1F/5M
3	V1	32	5	32 ± 5	3F/2M
4	V1	32	3	25 ± 2	1F/2M
5	V1	32	5	32 ± 6	4F/1M
6	V2	64	6	26 ± 6	2F/4M
7	V2	64	7	25 ± 3	6F/1M
8	V2	12	7	31 ± 5	3F/4M
9	V3	32	7	29 ± 3	4F/3M

multi-echo GRE sequence with whole-brain coverage was prescribed axially for each subject. Details on the acquisition parameters for each vendor defined by the SOPs are reported in Table 3. Both magnitude and phase images were collected on Philips and Siemens MRI systems, while on GE scanners we acquired the magnitude and the real and imaginary parts of the data which were used to produce phase images. In addition, a sagittal whole-brain 3D T1-weighted sequence with 1-mm isotropic resolution was acquired for anatomical reference.

Data processing

Susceptibility maps were computed using the algorithms implemented in STI Suite (MATLAB toolbox, available at https://people.eecs.berkeley.edu/~chunlei.liu/software.html from UC Berkeley, Berkeley, CA, USA) as follows. The raw phase images acquired at each echo were unwrapped using a Laplacian-based method [19,40]. The T2*-weighted image averaged across echoes was skull-stripped using Brain Extraction Toolbox (bet) [41] in FSL 5.0.9 (FMRIB Software Library, Oxford Centre for Functional MRI of the Brain, Oxford, UK) and the brain mask was used to remove the background field via V-SHARP [42]. Finally, we applied the iLSQR algorithm [43,44] to obtain QSM images for each echo that were then averaged to increase SNR [45].

The T1-weighted images were processed in FreeSurfer 6.0 [46,47] for brain extraction and for the parcellation of cortical regions and the segmentation of subcortical nuclei. The skull-stripped TE-averaged T2*-weighted image of each subject was aligned to the corresponding T1-weighted image via an affine transformation using antsRegistrationSyN routine in ANTs [48]. The computed transformation was then inverted and applied to the segmentation from which eight Regions Of Interest (ROI), each divided into left (L) and right (R) ROIs, were selected. Specifically, ROI-based analysis was performed in four subcortical regions, i.e. Caudate Nucleus (CN), Putamen (Pu), Globus Pallidus (GP) and Hippocampus (HC), and in four cortical areas, i.e. Cuneus (Cu), Precuneus (PCu), Precentral Gyrus (PCG) and Superior Frontal Gyrus (SFG).

Table 3
Acquisition parameters for 3D multi-echo GRE sequence of each vendor.

Vendor	Philips	Siemens	GE Healthcare
Sequence type	3D GR MULTIECHO FFE-3D	3D GRE (swi3d8r)	3D SWAN
FOV [mm]	224 × 224	224 × 224	224 × 224
Resolution [mm^3]	1 × 1 × 1	1 × 1 × 1	1 × 1 × 1
Matrix	224 × 224	224 × 224	224 × 224
Slice thickness [mm]	1	1	1
Slice gap [mm]	0	0	0
# slices	140	144	140
TR [ms]	40	51	51
Average TE [ms]	21	25.2	27.4
First TE [ms]	5.4	5.6	5.6
# echoes	7	8	7
Echo spacing [ms]	5.2	5.6	5.6
Flip angle (deg)	18	18	18
k-space coverage	–	6/8	0.85
Slice k-space coverage	–	6/8	–
Acceleration factor	SENSE = 2	GRAPPA = 2	ASSET = 2
Filter	CLEAR on	Prescan Normalize on	–
Bandwidth [Hz/px]	271	340	279
Duration [min]	≈ 8:11	≈ 8:45	≈ 8:01

For a voxel-wise analysis on traveling brain data, the TE-averaged T2*-weighted images of the same subject in different sites were co-registered via an affine transformation computed using antsRegistration in ANTs, which was then applied to susceptibility maps.

Statistical analysis

Statistical analysis was performed in MATLAB (MathWorks, Natick, MA, USA). Data from the traveling brain experiment were analyzed to assess inter-vendor reproducibility. A quantitative voxel-wise comparison was performed by computing structural similarity (SSIM) [49] using the ssim built-in function in MATLAB, and root-mean-squared error (RMSE) [50] as follows:

$$\mathrm{RMSE} = \sqrt{\sum_{i=1}^{n} \frac{(\chi_{1i} - \chi_{2i})^2}{n}}$$

where χ_{1i} and χ_{2i} indicate measured susceptibility for the i-th voxel at the two sites and n is the number of voxels. Estimation of SSIM and RMSE were provided both globally, i.e. by considering all the voxels in the brain mask, and locally by computing them in a moving 3 mm-radius region. In addition, we computed the voxel-wise difference (DIFF) between the two repeated scans.

Reproducibility evaluation was performed by computing an orthogonal linear fit and Pearson's correlation considering the susceptibility values in the voxels inside the brain mask for the scans performed at the two sites for each subject. An analogous ROI-based analysis was conducted after extracting average susceptibility and standard deviations from the selected ROIs. Via Bland-Altman plots, the mean difference and the 95 % limits of agreement were calculated for both voxel-wise and ROI-based analyses.

Cross-site variability of susceptibility measurements on a healthy population was performed considering average and standard deviation of susceptibility values for each ROI independently. Specifically, cross-subject variability within-site, within-vendor and cross-vendors were calculated via the between-subjects standard deviation for each ROI.

Results

Susceptibility maps for two exemplary subjects, one from area A1 and one from A2, scanned at two sites on scanners from two different vendors are shown in Fig. 1, together with the maps of SSIM and RMSE computed using a searchlight analysis approach, and the voxel-wise DIFF map. A global estimation of SSIM considering all the voxels in the brain mask yielded an across-subject average of 0.58 ± 0.11 and 0.60 ± 0.04 for A1 and A2 respectively, while the global RMSE was respectively 0.028 ± 0.005 ppm and 0.029 ± 0.0023 ppm. However, the computation of local SSIM and RMSE values highlighted that very low SSIM and high RMSE values are limited to particular regions, mainly located at the borders of the brain, at the skull base and at the edges of the cortex. Overall, high SSIM values were reached for both A1 and A2, with a median of 0.66 ± 0.09 and 0.65 ± 0.05 on average across subjects and a mode of 0.85 ± 0.08 and 0.72 ± 0.12 for A1 and A2 respectively. The median of RMSE distribution was 0.018 ± 0.004 ppm and 0.017 ± 0.002 ppm while the mode was 0.009 ± 0.002 ppm and 0.010 ± 0.003 ppm on average across subjects for A1 and A2 respectively.

The results of the voxelwise assessment of reproducibility are

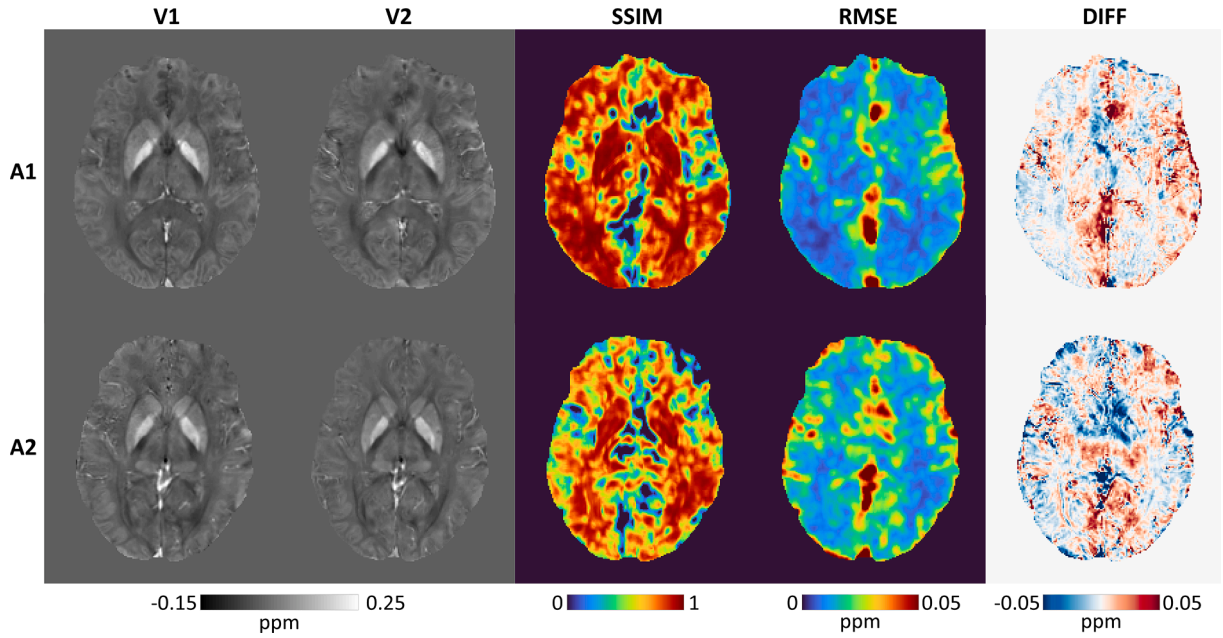

Fig. 1. Left panel: susceptibility maps obtained for two representative subjects scanned on the MRI platforms from vendors V1 and V2 of areas A1 and A2. Right panel: local estimation of SSIM and RMSE computed using a searchlight analysis approach and voxelwise difference map (DIFF).

reported in Table 4. Good Pearson's correlation was found and the orthogonal linear fit yielded angular coefficients close to 1, indicating high correspondence between χ values measured at the two sites, especially for A1, while the small intercepts indicate the absence of offset. No bias was reported in the Bland-Altman analysis and the 95 %-confidence intervals were $C.I._{A1} = 0.045 \pm 0.009$ ppm and $C.I._{A2} = 0.047 \pm 0.002$ ppm.

The results of the ROI-based analysis are reported in Table 4 and displayed in Fig. 2. High correlation between χ values measured on the scanner from V1 and V2 was observed in both A1 and A2 groups. The orthogonal linear fit yielded angular coefficients close to 1, indicating excellent reproducibility, though slightly lower for A2 than for A1. The subject-average difference between χ measures at the two sites ranged from 0.002 and 0.014 ppm with a median of 0.006 ppm for A1 depending on the ROI and from 0.001 to 0.017 ppm with a median of 0.007 ppm for A2. The Bland-Altman plots revealed the absence of biases and a 95 %-confidence interval C.I. = 0.02 ppm. However, for A2 a trend can be observed in susceptibility differences, being negative for negative χ and becoming positive for increasing χ.

Susceptibility values obtained for each ROI at each site are shown in Fig. 3. Cross-subject variability within-site was measured via the between-subjects standard deviation averaged across ROIs and ranged from 0.0064 ppm to 0.0083 ppm with a median of 0.0073 ppm. Cross-sites within-vendor variability was 0.0079 ppm, 0.0074 ppm and 0.0071 ppm for V1, V2 and V3 respectively on average across ROIs, while the average standard deviation across all sites and vendors was 0.0085 ppm. The average susceptibility for each ROI and the cross-vendor, within-vendor and within-site standard deviations are reported in Table 5. Fig. 4 shows the average susceptibility across the whole population and the susceptibility averaged across sites with MRI platforms from the same vendor with the corresponding standard deviations (See Table 5).

Table 4
Results for the reproducibility assessment in the traveling brain experiment obtained via voxelwise and ROI-based analysis. The angular coefficient and the intercept of the orthogonal linear fit, Pearson's correlation coefficient and Bland-Altman analysis parameters are reported.

		Voxelwise analysis		ROI-based analysis	
		A1	A2	A1	A2
Fit	Angular coefficient m	1.01 ± 0.05	0.77 ± 0.03	0.97	0.82
	Intercept q [ppm]	$(5 \pm 3)\cdot 10^{-4}$	$(13 \pm 4)\cdot 10^{-4}$	0.0013	0.0035
	Pearson's r	0.74 ± 0.08	0.69 ± 0.04	0.98	0.97
Bland-Altman	Mean difference [ppm]	$(-5 \pm 2)\cdot 10^{-4}$	$(-13 \pm 6)\cdot 10^{-4}$	$-4\cdot 10^{-4}$	$3\cdot 10^{-4}$
	95 % C.I. [ppm]	0.045 ± 0.009	0.047 ± 0.002	0.02	0.02

Discussion

In this work, we assessed the reproducibility of susceptibility maps obtained via QSM in a multicentric study at 3T using an optimized and harmonized protocol across MRI scanner platforms from three different vendors, consisting of a multi-echo GRE sequence with 1 mm isotropic spatial resolution. A traveling brain experiment was run on four different scanners from two vendors while nine sites collected data on groups of healthy volunteers to provide an estimation of the variability that can be expected in a multicentric multi-vendor study across a normative population.

The traveling brain experiment showed high SSIM (~ 0.8) and low RMSE (~ 0.01 ppm) of χ maps acquired on scanners from two different vendors across the whole brain, with some exceptions: areas at the border of the brain, at the skull base or near the interhemispheric or the transverse fissures suffer from the proximity to air-tissue interfaces or sinuses that may cause excessive phase wrap leading to incomplete dipole inversion, while χ comparisons at the edges of the cortex can be affected by registration errors. Excellent reproducibility was reported in both voxelwise and ROI-based analyses (m ~ 0.8–1). Voxelwise analysis yielded a good correlation (r ~ 0.7), partially affected by voxels in the previously mentioned areas showing higher RMSE, while excellent correlation (r ~ 1) was found in ROI-based analysis. Depending on the ROI, we reported inter-site χ differences of 0.001–0.017 ppm on average across participants in the traveling brain experiment. This is consistent with previous multi-sites reproducibility studies at 3T, reporting inter-site standard deviation of 0.006–0.012 ppm [37]. In addition, the 95

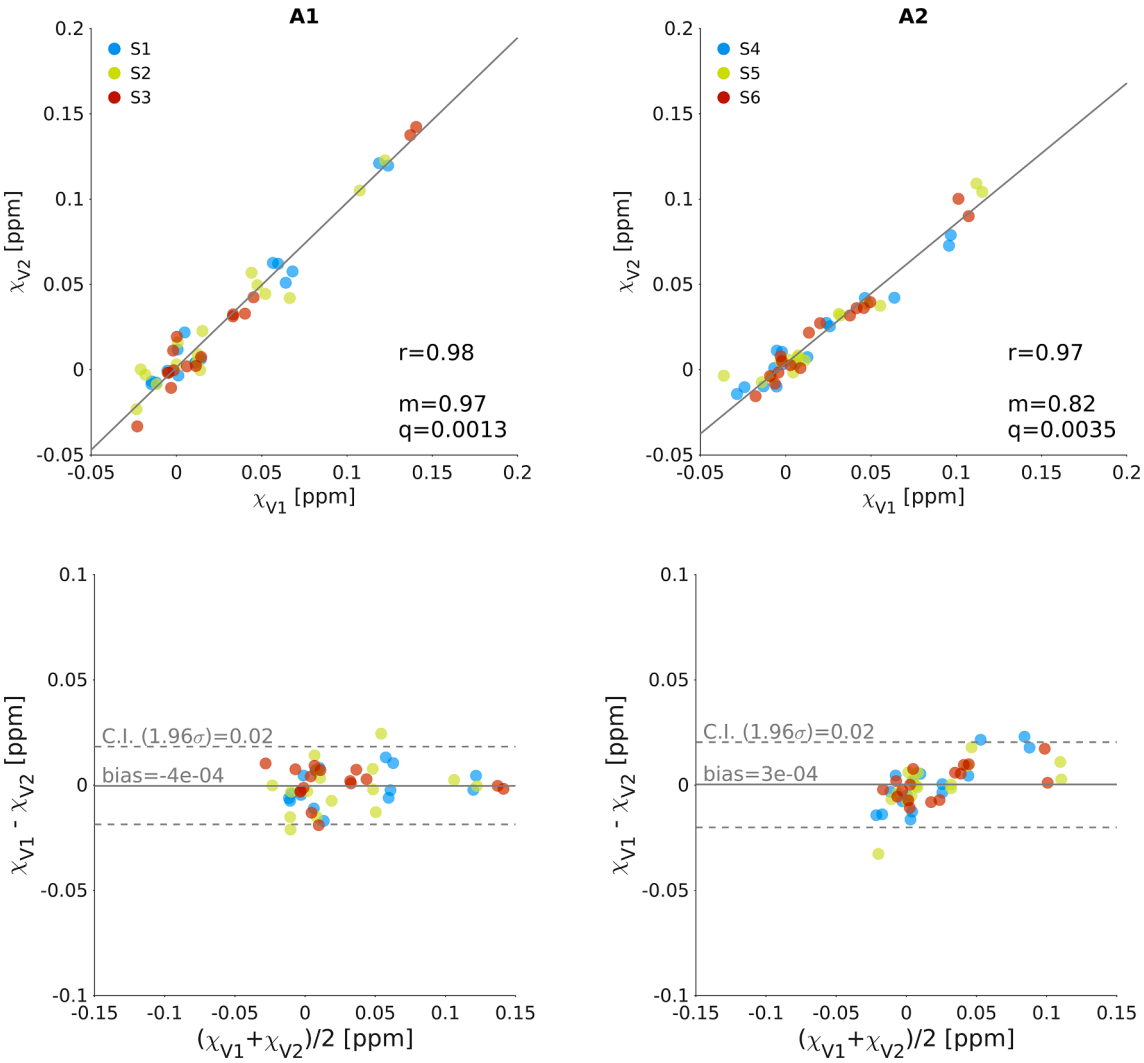

Fig. 2. Scatter plot (top row) and Bland-Altman plot (bottom row) of the ROI-based susceptibility measurement performed on scanners from vendors V1 and V2 in areas A1 (left column) and A2 (right column).

% C.I. (1.96 times the standard deviation) of 0.04 ppm and 0.02 ppm for voxelwise and ROI-based analysis are compatible with previously reported inter-vendor 95 % C.I. [36].

The within-site variability across subjects measured via the between-subjects standard deviation is slightly smaller on average than the inter-site within-vendor variability, which is in turn slightly smaller than the cross-vendor standard deviation. However, the variability estimations are very similar, being of the order of 0.01 ppm for deep gray matter nuclei except for HC, and of the order of 0.005 ppm for cortical regions and HC, even though the scanners involved in the study are equipped with different hardware and operate with different software versions, even when they refer to the same vendor. These calculations were performed on separated cohorts of healthy subjects which differed from one site to the other rather than a group of traveling brains, so taking into account the physiological variance observable for different subjects and reproducing more realistically the conditions of a multicentric study. Despite this additional contribution to the variance, both the within-site and cross-site variability are comparable to the standard deviation obtained by the Bland-Altman analysis on the traveling brain data and to what was reported in previous traveling brain studies [36,37].

The QSM acquisition protocol implemented in this study was set up using product pulse sequences already installed on the MRI systems, with no additional programming required, and the reconstruction algorithms provided by the vendors in order to be able to easily export the protocol to other clinical hospitals or research centers and extend or create new multicenter networks. The drawback for portability is that the acquisition is not locally-optimized and may not represent the most performing option at a particular site. The sequence used in this study had an acceptable but slightly long acquisition time (~ 8–9 min). However, some acceleration approaches such as compressed sensing were not available at all sites and are not widely spread in clinical settings, so they were not employed in this work. The spatial resolution obtained with this protocol may serve many clinical aims, but partial volume effect may limit studies targeting small subcortical structures such as nigrosome 1 or locus coeruleus. In this study we chose to use a well-established QSM pipeline [51–54]. As different pipelines produce slightly different quantitative results [55], it is critical to standardize the QSM reconstruction pipeline when pooling data from different sites.

QSM cannot quantify susceptibility in absolute terms, but only with respect to a reference value, due to an unknown region-independent offset [56,57]. Susceptibility measures should be then referred to a reference region. Criteria for reference region selection include easy delineation and segmentation, susceptibility ideally not affected by age, head orientation or disease condition. Several candidate brain regions have been suggested [58,59], such as frontal white matter, internal capsule, cerebrospinal fluids (CSF) in ventricles and the whole brain. However, measured susceptibility white matter tracts may be influenced by head orientation [19–22], while the ventricles do not only contain

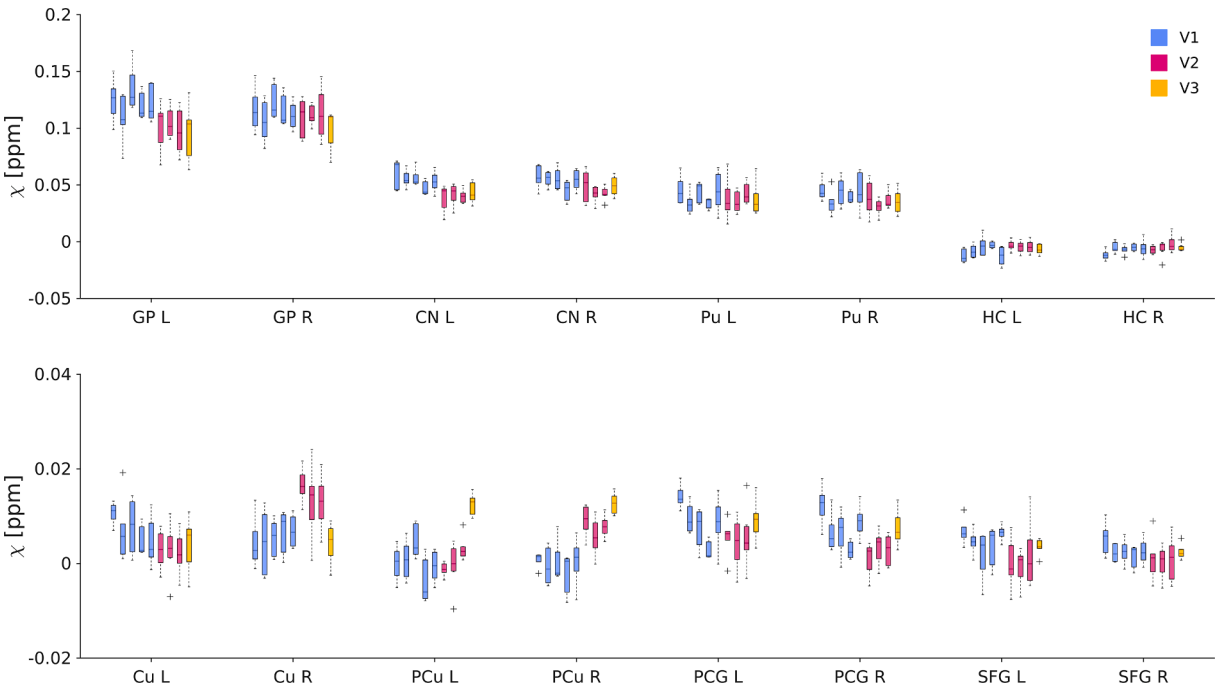

Fig. 3. Susceptibility values obtained for each ROI at each site. The first five blue boxes refer to sites equipped with MRI systems from vendor V1, the following three pink boxes from vendor V2, and the last yellow box from vendor V3. The bottom and top edges of each box indicate the 25th and 75th percentile respectively of the susceptibility distribution at each site for a particular ROI and the central line indicates the median. The whiskers extend to the maximum and minimum values excluding outliers, which are plotted using the '+' symbol.

Table 5
Susceptibility values and standard deviations measured on groups of healthy controls. As only one scanner from vendor V3 was available in this study, the within-vendor standard deviation for V3 coincides with the within-site estimation of QSM variability.

Susceptibility values [ppm]								
ROI	**Cross-vendor**		**Within-vendor**			**Within-site**		
	Mean	Std	V1 std	V2 std	V3 std	Min std	Max std	Mean std
GP L	0.110	0.022	0.019	0.017	0.024	0.013	0.024	0.019
GP R	0.111	0.017	0.016	0.016	0.017	0.008	0.022	0.016
CN L	0.048	0.011	0.009	0.008	0.009	0.006	0.013	0.009
CN R	0.050	0.010	0.009	0.009	0.008	0.006	0.014	0.009
Pu L	0.039	0.012	0.012	0.012	0.013	0.006	0.018	0.012
Pu R	0.038	0.011	0.012	0.010	0.010	0.006	0.017	0.011
HC L	−0.0065	0.0064	0.0075	0.0048	0.0044	0.0034	0.0090	0.0057
HC R	−0.0060	0.0056	0.0055	0.0063	0.0034	0.0034	0.0080	0.0052
Cu L	0.0050	0.0053	0.0052	0.0044	0.0054	0.0024	0.0066	0.0048
Cu R	0.0087	0.0067	0.0048	0.0057	0.0041	0.0034	0.0073	0.0050
PCu L	0.0022	0.0056	0.0044	0.0036	0.0022	0.0014	0.0058	0.0035
PCu R	0.0046	0.0058	0.0038	0.0033	0.0022	0.0016	0.0052	0.0035
PCG L	0.0075	0.0051	0.0047	0.0049	0.0040	0.0024	0.0060	0.0041
PCG R	0.0056	0.0047	0.0047	0.0033	0.0035	0.0022	0.0048	0.0036
SFG L	0.0028	0.0046	0.0037	0.0051	0.0016	0.0016	0.0067	0.0038
SFG R	0.0020	0.0033	0.0028	0.0039	0.0015	0.0015	0.0046	0.0031

CSF and the presence of veins and choroid plexus can alter susceptibility. Moreover, ventricles are typically small in young healthy subjects and their susceptibility may be affected by partial volume effect. These factors make the delineation of an ROI in the ventricles complex and operator-dependent. Previous studies reported that whole-brain referencing reduces cross-site and within-site QSM variability with respect to CSF referencing [38] and that the referencing operation represents a small adjustment compared to other factors such as age [60]. For this reason, as the QSM processing pipeline used in this study sets to zero the average susceptibility in the whole brain mask, we left measured χ values unreferenced. Similarly, the ROI-based analysis was performed using automatic segmentations of deep gray matter nuclei and automatic cortical parcellations performed on the T1-weighted images to eliminate operator-dependent bias.

The harmonization across MRI systems from different vendors was not trivial and different sequence implementations led to different echo trains. As matching TEs is crucial to achieve reproducibility [29], we aimed at having the first TE, the average TE and the train length uniform at all sites. As shown in Table 3, the first TE and the average TE were similar, though not the same, across vendors, with the largest difference being 6.4 ms between average TE for Philips and GE. Moreover, eight echoes were acquired on Siemens scanners, while seven were acquired on Philips and GE. This can lead to differences in signal-to-noise ratio of the average susceptibility map.

Limitations to the traveling brain experiment may relate to the small sample size and to the lack of test–retest repeatability assessment on the

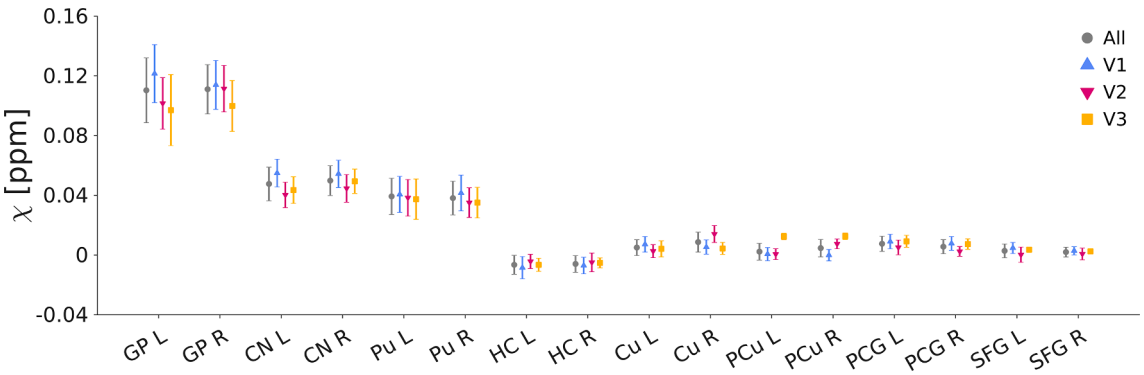

Fig. 4. Average susceptibility values and corresponding standard deviations. The gray dots represent the mean of the whole cohort of subjects across all sites, while the triangles and the square markers indicate average susceptibility values measured on average across sites from each of the three vendors.

same scanner. Moreover, scanners from only two vendors were involved. However, the consistency of the results across subjects, across the two areas A1 and A2 and the correspondence with what has previously been reported in the literature [36,37] support the reliability of findings. Also the second part of the study concerning the estimation of QSM variability cross-sites in a healthy population is limited by the small population acquired at each site. Moreover, only one site with an MR system from vendor V3 was involved in the study. This should be considered when comparing the within-vendor standard deviations in Table 5, as for V3 it actually represents a within-site cross-subjects variability. It should be also taken into account that the standard deviation between different sites with systems from the same vendor can be affected by different scanner models, software releases and coils (see Table 1). Subject age might be another possible confounding factor, as some brain areas are known to accumulate iron due to aging [60,61]. For this reason, we enrolled young and healthy subjects in a narrow age interval, equally distributed across sites.

This study supports the effective feasibility of the potential use of QSM in multicentric studies evaluating within-site and cross-site reproducibility and repeatability. In future works, the RIN – Neuroimaging Network will enroll populations of patients with well-known patterns of susceptibility alteration, e.g. patients with dementia [15,62,63], Parkinson's disease [64,65], multiple sclerosis and white matter disease [32,66–68], and an age-matched cohort of healthy subjects in order to compare the within-site and the cross-site performance of QSM in discriminating the two groups, so evaluating the effective feasibility and sensitivity of multicentric studies.

In conclusion, we implemented and optimized a harmonized protocol for QSM across 3T MRI scanner platforms from three different vendors. Importantly, we leveraged product sequences and signal reconstruction algorithms provided by the vendor, to set a protocol easy to implement on clinical scanners. Despite some differences in the acquisition parameters due to slightly different sequence implementations for each vendor, we obtained excellent reproducibility in the traveling brain experiment. We provided an ROI-dependent estimation of the variability of susceptibility measurements that could be expected in a healthy population in a multicentric study and reported a precision of the order of 0.005–0.025 ppm. Hence, we suggest that multicentric multi-vendor studies using QSM at 3T are feasible and reliable in quantifying magnetic susceptibility in both cortical and subcortical gray matter regions.

The RIN–Neuroimaging Network

Alberto Redolfi (IRCCS Istituto Centro San Giovanni di Dio Fatebenefratelli), Egidio D'Angelo (Fondazione IRCCS Istituto Neurologico Naz.le Mondino, University of Pavia), Gianluigi Forloni (Istituto di Ricerche Farmacologiche Mario Negri IRCCS), Raffaele Agati (IRCCS Istituto delle Scienze Neurologiche di Bologna), Marco Aiello (IRCCS SDN Istituto di Ricerca), Elisa Alberici (IRCCS Istituti Clinici Scientifici Maugeri), Carmelo Amato (Oasi Research Institute-IRCCS), Filippo Arrigoni (Istituto Scientifico, IRCCS E. Medea), Francesca Baglio (IRCCS Fondazione don Carlo Gnocchi onlus), Stefano Bastianello (Fondazione IRCCS Istituto Neurologico Naz.le Mondino), Lilla Bonanno (IRCCS Centro Neurolesi Bonino Pulejo), Francesca Bottino (IRCCS Istituto Ospedale Pediatrico Bambino Gesù), Marco Bozzali (Fondazione IRCCS Santa Lucia), Chiara Carducci (IRCCS Istituto Ospedale Pediatrico Bambino Gesù), Lorenzo Carnevale (IRCCS Neuromed), Antonella Castellano (IRCCS Ospedale San Raffaele), Carlo Cavaliere (IRCCS SDN Istituto di Ricerca), Mattia Colnaghi (Istituto Auxologico Italiano IRCCS), Giorgio Conte (Fondazione IRCCS Ca' Granda Osp. Maggiore Policlinico), Silvia De Francesco (IRCCS Istituto Centro San Giovanni di Dio Fatebenefratelli), Greta Demichelis (Fondazione IRCCS Istituto Neurologico Carlo Besta), Valeria Elisa Contarino (Fondazione IRCCS Ca' Granda Osp. Maggiore Policlinico), Andrea Falini (IRCCS Ospedale San Raffaele), Giulio Ferrazzi (IRCCS Ospedale San Camillo), Lorenzo Figà Talamanca (IRCCS Istituto Ospedale Pediatrico Bambino Gesù), Cira Fundarò (IRCCS Istituti Clinici Scientifici Maugeri), Simona Gaudino (IRCCS Fondazione Policlinico Universitario Agostino Gemelli), Francesco Ghielmetti (Fondazione IRCCS Istituto Neurologico Carlo Besta), Ruben Gianeri (Fondazione IRCCS Istituto Neurologico Carlo Besta), Marco Grimaldi (IRCCS Istituto Clinico Humanitas), Antonella Iadanza (IRCCS Ospedale San Raffaele), Fabrizio Levrero (IRCCS Ospedale Policlinico San Martino), Raffaele Lodi (IRCCS Istituto delle Scienze Neurologiche di Bologna), Daniela Longo (IRCCS Istituto Ospedale Pediatrico Bambino Gesù), Giulia Lucignani (IRCCS Istituto Ospedale Pediatrico Bambino Gesù), Martina Lucignani (IRCCS Istituto Ospedale Pediatrico Bambino Gesù), Maria Luisa Malosio (IRCCS Istituto Clinico Humanitas), Vittorio Manzo (Istituto Auxologico Italiano, IRCCS), M. Marcella Laganà (IRCCS Fondazione don Carlo Gnocchi onlus), Silvia Marino (IRCCS Centro Neurolesi Bonino Pulejo), Jean Paul Medina (Fondazione IRCCS Istituto Neurologico Carlo Besta), Edoardo Micotti (Istituto di Ricerche Farmacologiche Mario Negri IRCCS), Claudia Morelli (Istituto Auxologico Italiano IRCCS), Alessio Moscato (IRCCS Istituti Clinici Scientifici Maugeri), Francesco Padelli (Fondazione IRCCS Istituto Neurologico Carlo Besta), Sara Palermo (Fondazione IRCCS Istituto Neurologico Carlo Besta), Patrizia Pantano (RCCS Neuromed), Chiara Parrillo (IRCCS Istituto Ospedale Pediatrico Bambino Gesù), Denis Peruzzo (Istituto Scientifico, IRCCS E. Medea), Nikolaos Petsas (IRCCS Neuromed), Letterio S. Politi (IRCCS Istituto Clinico Humanitas), Luca Roccatagliata (IRCCS Ospedale Policlinico San Martino), Elisa Rognone (Fondazione IRCCS Istituto Neurologico Naz.le Mondino), Andrea Rossi (Ospedale Pediatrico Istituto Giannina Gaslini, Università di Genova), Maria Camilla Rossi-Espagnet (IRCCS Istituto Ospedale Pediatrico Bambino Gesù), Claudia Ruvolo (IRCCS Centro Neurolesi Bonino Pulejo), Marco Salvatore (IRCCS SDN Istituto di Ricerca), Emanuela Tagliente (IRCCS Istituto Ospedale Pediatrico Bambino Gesù), Claudia Testa (IRCCS Istituto delle Scienze

Neurologiche di Bologna), Caterina Tonon (IRCCS Istituto delle Scienze Neurologiche di Bologna), Domenico Tortora (Ospedale Pediatrico Istituto Giannina Gaslini), Fabio Maria Triulzi (Fondazione IRCCS Ca' Granda Osp. Maggiore Policlinico).

Declaration of Competing Interest

The authors declare that they have no known competing financial interests or personal relationships that could have appeared to influence the work reported in this paper.

Acknowledgements

This project was funded by the Italian Minister of Health (RRC-2016-2361095, RRC-2017-2364915, RRC-2018-2365796, and RCR-2019-23669119_001, RCR 2020-23670067, and RCR-2022-23682285) and the Ministry of Economy and Finance (CCR-2017-23669078). This study was also partially supported by grant RC and the 5x1000 voluntary contributions to IRCCS Fondazione Stella Maris, funded by the Italian Ministry of Health. The funding sources had no role in the design and conduct of the study; in the collection, analysis, and interpretation of the data; or in the preparation, review, and approval of the manuscript.

References

[1] Ndayisaba A, Kaindlstorfer C, Wenning GK. Iron in Neurodegeneration – Cause or Consequence? Front Neurosci 2019;13. https://doi.org/10.3389/fnins.2019.00180.
[2] Ward RJ, Zucca FA, Duyn JH, Crichton RR, Zecca L. The role of iron in brain ageing and neurodegenerative disorders. Lancet Neurol 2014;13:1045–60. https://doi.org/10.1016/S1474-4422(14)70117-6.
[3] de Rochefort L, Liu T, Kressler B, Liu J, Spincemaille P, Lebon V, et al. Quantitative susceptibility map reconstruction from MR phase data using bayesian regularization: validation and application to brain imaging. Magn Reson Med 2010;63(1):194–206. https://doi.org/10.1002/mrm.22187.
[4] Li L, Leigh JS. Quantifying arbitrary magnetic susceptibility distributions with MR. Magn Reson Med 2004;51:1077–82. https://doi.org/10.1002/mrm.20054.
[5] Wharton S, Schäfer A, Bowtell R. Susceptibility mapping in the human brain using threshold-based k-space division. Magn Reson Med 2010;63:1292–304. https://doi.org/10.1002/mrm.22334.
[6] Ravanfar P, Loi SM, Syeda WT, Van Rheenen TE, Bush AI, Desmond P, et al. Systematic review: quantitative susceptibility mapping (QSM) of brain iron profile in neurodegenerative diseases. Front Neurosci 2021;15. https://doi.org/10.3389/fnins.2021.618435.
[7] Vinayagamani S, Sheelakumari R, Sabarish S, Senthilvelan S, Ros R, Thomas B, et al. Quantitative susceptibility mapping: technical considerations and clinical applications in neuroimaging. J Magn Reson Imaging 2021;53(1):23–37. https://doi.org/10.1002/jmri.27058.
[8] Acosta-Cabronero J, Cardenas-Blanco A, Betts MJ, Butryn M, Valdes-Herrera JP, Galazky I, et al. The whole-brain pattern of magnetic susceptibility perturbations in Parkinson's disease. Brain 2017;140(1):118–31. https://doi.org/10.1093/brain/aww278.
[9] Biondetti E, Santin MD, Valabrègue R, Mangone G, Gaurav R, Pyatigorskaya N, et al. The spatiotemporal changes in dopamine, neuromelanin and iron characterizing Parkinson's disease. Brain 2021;144. https://doi.org/10.1093/brain/awab191.
[10] Pyatigorskaya N, Sanz-Morère CB, Gaurav R, Biondetti E, Valabregue R, Santin M, et al. Iron imaging as a diagnostic tool for parkinson's disease: a systematic review and meta-analysis. Front Neurol 2020;11:366. https://doi.org/10.3389/fneur.2020.00366.
[11] Lancione M, Donatelli G, Del Prete E, Campese N, Frosini D, Cencini M, et al. Evaluation of iron overload in nigrosome 1 via quantitative susceptibility mapping as a progression biomarker in prodromal stages of synucleinopathies. NeuroImage 2022;260:119454. https://doi.org/10.1016/j.neuroimage.2022.119454.
[12] Acosta-Cabronero J, Machts J, Schreiber S, Abdulla S, Kollewe K, Petri S, et al. Quantitative susceptibility MRI to detect brain iron in amyotrophic lateral sclerosis. Radiology 2018;289(1):195–203. https://doi.org/10.1148/radiol.2018180112.
[13] Costagli M, Symms MR, Angeli L, Kelley DAC, Biagi L, Farnetani A, et al. Assessment of silent T1-weighted head imaging at 7 T. Eur Radiol 2016;26:1879–88. https://doi.org/10.1007/s00330-015-3954-2.
[14] Wang C, Foxley S, Ansorge O, Bangerter-Christensen S, Chiew M, Leonte A, et al. Methods for quantitative susceptibility and R2* mapping in whole post-mortem brains at 7T applied to amyotrophic lateral sclerosis. NeuroImage 2020;222:117216. https://doi.org/10.1016/j.neuroimage.2020.117216.
[15] Acosta-Cabronero J, Williams GB, Cardenas-Blanco A, Arnold RJ, Lupson V, Nestor PJ, et al. In Vivo quantitative susceptibility mapping (QSM) in Alzheimer's disease. PLoS ONE 2013;8(11):e81093. https://doi.org/10.1371/journal.pone.0081093.
[16] Ayton S, Fazlollahi A, Bourgeat P, Raniga P, Ng A, Lim YY, et al. Cerebral quantitative susceptibility mapping predicts amyloid-β-related cognitive decline. Brain 2017;140(8):2112–9. https://doi.org/10.1093/brain/awx137.
[17] Cogswell PM, Wiste HJ, Senjem ML, Gunter JL, Weigand SD, Schwarz CG, et al. Associations of quantitative susceptibility mapping with Alzheimer's disease clinical and imaging markers. NeuroImage 2021;224:117433. https://doi.org/10.1016/j.neuroimage.2020.117433.
[18] Kim H-G, Park S, Rhee HY, Lee KM, Ryu C-W, Rhee SJ, et al. Quantitative susceptibility mapping to evaluate the early stage of Alzheimer's disease. NeuroImage Clin 2017;16:429–38. https://doi.org/10.1016/j.nicl.2017.08.019.
[19] Li W, Wu B, Avram AV, Liu C. Magnetic susceptibility anisotropy of human brain in vivo and its molecular underpinnings. NeuroImage 2012;59:2088–97. https://doi.org/10.1016/j.neuroimage.2011.10.038.
[20] Liu C, Li W, Johnson GA, Wu B. High-field (9.4T) MRI of brain dysmyelination by quantitative mapping of magnetic susceptibility. NeuroImage 2011;56(3):930–8. https://doi.org/10.1016/j.neuroimage.2011.02.024.
[21] Wharton S, Bowtell R. Effects of white matter microstructure on phase and susceptibility maps. Magn Reson Med 2015;73:1258–69. https://doi.org/10.1002/mrm.25189.
[22] Lancione M, Tosetti M, Donatelli G, Cosottini M, Costagli M. The impact of white matter fiber orientation in single-acquisition quantitative susceptibility mapping. NMR Biomed 2017;30(11):e3798. https://doi.org/10.1002/nbm.3798.
[23] Karsa A, Punwani S, Shmueli K. The effect of low resolution and coverage on the accuracy of susceptibility mapping. Magn Reson Med 2018;81:1833–48. https://doi.org/10.1002/mrm.27542.
[24] Zhou D, Cho J, Zhang J, Spincemaille P, Wang Y. Susceptibility underestimation in a high-susceptibility phantom: dependence on imaging resolution, magnitude contrast, and other parameters. Magn Reson Med 2017;78:1080–6. https://doi.org/10.1002/mrm.26475.
[25] Elkady AM, Sun H, Wilman AH. Importance of extended spatial coverage for quantitative susceptibility mapping of iron-rich deep gray matter. Magn Reson Imaging 2016;34:574–8. https://doi.org/10.1016/J.MRI.2015.12.032.
[26] Biondetti E, Karsa A, Thomas DL, Shmueli K. Investigating the accuracy and precision of TE-dependent versus multi-echo QSM using Laplacian-based methods at 3 T. Magn Reson Med 2020;84:3040–53. https://doi.org/10.1002/mrm.28331.
[27] Cronin MJ, Wang N, Decker KS, Wei H, Zhu W-Z, Liu C. Exploring the origins of echo-time-dependent quantitative susceptibility mapping (QSM) measurements in healthy tissue and cerebral microbleeds. NeuroImage 2017;149:98–113. https://doi.org/10.1016/j.neuroimage.2017.01.053.
[28] Lancione M, Cencini M, Costagli M, Donatelli G, Tosetti M, Giannini G, et al. Diagnostic accuracy of quantitative susceptibility mapping in multiple system atrophy: the impact of echo time and the potential of histogram analysis. NeuroImage Clin 2022;34:102989. https://doi.org/10.1016/j.nicl.2022.102989.
[29] Lancione M, Donatelli G, Cecchi P, Cosottini M, Tosetti M, Costagli M. Echo-time dependency of quantitative susceptibility mapping reproducibility at different magnetic field strengths. NeuroImage 2019;197:557–64. https://doi.org/10.1016/j.neuroimage.2019.05.004.
[30] Sood S, Urriola J, Reutens D, O'Brien K, Bollmann S, Barth M, et al. Echo time-dependent quantitative susceptibility mapping contains information on tissue properties. Magn Reson Med 2017;77(5):1946–58. https://doi.org/10.1002/mrm.26281.
[31] Spincemaille P, Anderson J, Wu G, Yang B, Fung M, Li Ke, et al. Quantitative susceptibility mapping: MRI at 7T versus 3T. J Neuroimaging 2020;30(1):65–75. https://doi.org/10.1111/jon.12669.
[32] Emmerich J, Bachert P, Ladd ME, Straub S. On the separation of susceptibility sources in quantitative susceptibility mapping: theory and phantom validation with an in vivo application to multiple sclerosis lesions of different age. J Magn Reson 2021;330:107033. https://doi.org/10.1016/J.JMR.2021.107033.
[33] Hinoda T, Fushimi Y, Okada T, Fujimoto K, Liu C, Yamamoto A, et al. Quantitative susceptibility mapping at 3 T and 1.5 T. Invest Radiol 2015;50(8):522–30. https://doi.org/10.1097/RLI.0000000000000159.
[34] Voelker MN, Kraff O, Goerke S, Laun FB, Hanspach J, Pine KJ, et al. The traveling heads 2.0: multicenter reproducibility of quantitative imaging methods at 7 Tesla. NeuroImage 2021;232:117910. https://doi.org/10.1016/j.neuroimage.2021.117910.
[35] Wang R, Xie G, Zhai M, Zhang Z, Wu B, Zheng D, et al. Stability of R2* and quantitative susceptibility mapping of the brain tissue in a large scale multi-center study. Sci Rep 2017;7(1). https://doi.org/10.1038/srep45261.
[36] Deh K, Nguyen TD, Eskreis-Winkler S, Prince MR, Spincemaille P, Gauthier S, et al. Reproducibility of quantitative susceptibility mapping in the brain at two field strengths from two vendors. J Magn Reson Imaging 2015;42(6):1592–600. https://doi.org/10.1002/jmri.24943.
[37] Lin P-Y, Chao T-C, Wu M-L. Quantitative susceptibility mapping of human brain at 3T: a multisite reproducibility study. Am J Neuroradiol 2015;36:467–74. https://doi.org/10.3174/ajnr.A4137.
[38] Rua C, Clarke WT, Driver ID, Mougin O, Morgan AT, Clare S, et al. Multi-centre, multi-vendor reproducibility of 7T QSM and R2* in the human brain: results from the UK7T study. NeuroImage 2020;223:117358. https://doi.org/10.1016/j.neuroimage.2020.117358.
[39] Nigri A, Ferraro S, Gandini Wheeler-Kingshott CA, Tosetti M, Redolfi A, Forloni G, et al. Quantitative MRI harmonization to maximize clinical impact: the RIN–Neuroimaging Network. Front Neurol 2022;13:855125. https://doi.org/10.3389/fneur.2022.855125.

[40] Schofield MA, Zhu Y. Fast phase unwrapping algorithm for interferometric applications. Opt Lett 2003;28:1194–6. https://doi.org/10.1364/OL.28.001194.
[41] Smith SM. Fast robust automated brain extraction. Hum Brain Mapp 2002;17:143–55. https://doi.org/10.1002/hbm.10062.
[42] Schweser F, Deistung A, Lehr BW, Reichenbach JR. Quantitative imaging of intrinsic magnetic tissue properties using MRI signal phase: an approach to in vivo brain iron metabolism? NeuroImage 2011;54:2789–807. https://doi.org/10.1016/j.neuroimage.2010.10.070.
[43] Li W, Wang N, Yu F, Han H, Cao W, Romero R, et al. A method for estimating and removing streaking artifacts in quantitative susceptibility mapping. NeuroImage 2015;108:111–22. https://doi.org/10.1016/j.neuroimage.2014.12.043.
[44] Li W, Wu B, Liu C. Quantitative susceptibility mapping of human brain reflects spatial variation in tissue composition. NeuroImage 2011;55:1645–56. https://doi.org/10.1016/j.neuroimage.2010.11.088.
[45] Denk C, Rauscher A. Susceptibility weighted imaging with multiple echoes. J Magn Reson Imaging 2010;31:185–91. https://doi.org/10.1002/jmri.21995.
[46] Desikan RS, Ségonne F, Fischl B, Quinn BT, Dickerson BC, Blacker D, et al. An automated labeling system for subdividing the human cerebral cortex on MRI scans into gyral based regions of interest. NeuroImage 2006;31(3):968–80. https://doi.org/10.1016/j.neuroimage.2006.01.021.
[47] Fischl B, Salat DH, Busa E, Albert M, Dieterich M, Haselgrove C, et al. Whole brain segmentation: automated labeling of neuroanatomical structures in the human brain. Neuron 2002;33(3):341–55. https://doi.org/10.1016/S0896-6273(02)00569-X.
[48] Avants BB, Epstein CL, Grossman M, Gee JC. Symmetric diffeomorphic image registration with cross-correlation: evaluating automated labeling of elderly and neurodegenerative brain. Med Image Anal 2008;12:26–41. https://doi.org/10.1016/j.media.2007.06.004.
[49] Wang Z, Bovik AC, Sheikh HR, Simoncelli EP. Image quality assessment: from error visibility to structural similarity. IEEE Trans Image Process 2004;13:600–12. https://doi.org/10.1109/TIP.2003.819861.
[50] Langkammer C, Schweser F, Shmueli K, Kames C, Li Xu, Guo Li, et al. Quantitative susceptibility mapping: report from the 2016 reconstruction challenge. Magn Reson Med 2018;79(3):1661–73. https://doi.org/10.1002/mrm.26830.
[51] Costagli M, Donatelli G, Cecchi P, Bosco P, Migaleddu G, Siciliano G, et al. Distribution indices of magnetic susceptibility values in the primary motor cortex enable to classify patients with amyotrophic lateral sclerosis. Brain Sci 2022;12(7):942. https://doi.org/10.3390/brainsci12070942.
[52] Howard CM, Jain S, Cook AD, Packard LE, Mullin HA, Chen N, et al. Cortical iron mediates age-related decline in fluid cognition. Hum Brain Mapp 2022;43:1047–60. https://doi.org/10.1002/hbm.25706.
[53] Monti S, Pontillo G, Russo C, Cella L, Cocozza S, Palma G. RESUMEN: a flexible class of multi-parameter qMRI protocols. Phys Medica Eur J Med Phys 2021;88:23–36. https://doi.org/10.1016/j.ejmp.2021.04.005.
[54] Ward PGD, Harding IH, Close TG, Corben LA, Delatycki MB, Storey E, et al. Longitudinal evaluation of iron concentration and atrophy in the dentate nuclei in friedreich ataxia. Mov Disord 2019;34(3):335–43. https://doi.org/10.1002/mds.27606.
[55] Bilgic B, Langkammer C, Marques JP, Meineke J, Milovic C, Schweser F. QSM reconstruction challenge 2.0: Design and report of results. Magn Reson Med 2021;86(3):1241–55. https://doi.org/10.1002/mrm.28754.
[56] Cheng YCN, Neelavalli J, Haacke EM. Limitations of calculating field distributions and magnetic susceptibilities in MRI using a Fourier based method. Phys Med Biol 2009;54:1169–89. https://doi.org/10.1088/0031-9155/54/5/005.
[57] Koch KM, Papademetris X, Rothman DL, De Graaf RA. Rapid calculations of susceptibility-induced magnetostatic field perturbations for in vivo magnetic resonance. Phys Med Biol 2006;51:6381–402. https://doi.org/10.1088/0031-9155/51/24/007.
[58] Feng X, Deistung A, Reichenbach JR. Quantitative susceptibility mapping (QSM) and R2* in the human brain at 3 T: evaluation of intra-scanner repeatability. Z Für Med Phys 2018;28(1):36–48. https://doi.org/10.1016/j.zemedi.2017.05.003.
[59] Straub S, Schneider TM, Emmerich J, Freitag MT, Ziener CH, Schlemmer H-P, et al. Suitable reference tissues for quantitative susceptibility mapping of the brain. Magn Reson Med 2017;78(1):204–14. https://doi.org/10.1002/mrm.26369.
[60] Acosta-Cabronero J, Betts MJ, Cardenas-Blanco A, Yang S, Nestor PJ. In Vivo MRI Mapping of brain iron deposition across the adult lifespan. Neurobiol Dis 2016;36:364–74. https://doi.org/10.1523/JNEUROSCI.1907-15.2016.
[61] Betts MJ, Acosta-Cabronero J, Cardenas-Blanco A, Nestor PJ, Düzel E. High-resolution characterisation of the aging brain using simultaneous quantitative susceptibility mapping (QSM) and R2* measurements at 7 T. NeuroImage 2016;138:43–63. https://doi.org/10.1016/j.neuroimage.2016.05.024.
[62] Tiepolt S, Schäfer A, Rullmann M, Roggenhofer E, Gertz H-J, Schroeter ML, et al. Quantitative susceptibility mapping of amyloid-β aggregates in Alzheimer's disease with 7T MR. J Alzheimers Dis 2018;64(2):393–404. https://doi.org/10.3233/JAD-180118.
[63] Tuzzi E, Balla DZ, Loureiro JRA, Neumann M, Laske C, Pohmann R, et al. Ultra-high field MRI in Alzheimer's disease: effective transverse relaxation rate and quantitative susceptibility mapping of human brain in vivo and ex vivo compared to histology. J Alzheimers Dis JAD 2020;73(4):1481–99. https://doi.org/10.3233/JAD-190424.
[64] Barbosa JHO, Santos AC, Tumas V, Liu M, Zheng W, Haacke EM, et al. Quantifying brain iron deposition in patients with Parkinson's disease using quantitative susceptibility mapping, R2 and R2*. Magn Reson Imaging 2015;33(5):559–65. https://doi.org/10.1016/j.mri.2015.02.021.
[65] Langkammer C, Pirpamer L, Seiler S, Deistung A, Schweser F, Franthal S, et al. Quantitative susceptibility mapping in Parkinson's disease. PLoS ONE 2016;11(9):e0162460. https://doi.org/10.1371/journal.pone.0162460.
[66] Deh K, Ponath GD, Molvi Z, Parel G-C, Gillen KM, Zhang S, et al. Magnetic susceptibility increases as diamagnetic molecules breakdown: Myelin digestion during multiple sclerosis lesion formation contributes to increase on QSM. J Magn Reson Imaging 2018;48(5):1281–7. https://doi.org/10.1002/jmri.25997.
[67] Shin H-G, Lee J, Yun YH, Yoo SH, Jang J, Oh S-H, et al. χ-separation: magnetic susceptibility source separation toward iron and myelin mapping in the brain. NeuroImage 2021;240:118371. https://doi.org/10.1016/j.neuroimage.2021.118371.
[68] Wisnieff C, Ramanan S, Olesik J, Gauthier S, Wang Y, Pitt D. Quantitative susceptibility mapping (QSM) of white matter multiple sclerosis lesions: interpreting positive susceptibility and the presence of iron. Magn Reson Med 2015;74:564–70. https://doi.org/10.1002/mrm.25420.